Rock and Soil Mechanics

Volume 42 | Issue 12 Article 6

2-28-2022

The phase field numerical manifold method for crack propagation in rock

Liang YANG
University of Chinese Academy of Sciences, Beijing 100049, China

Yong-tao YANG
State Key Laboratory of Geomechanics and Geotechnical Engineering, Institute of Rock and Soil Mechanics, Chinese Academy of Sciences, Wuhan, Hubei 430071, China

Hong ZHENG
Key Laboratory of Urban Security and Disaster Engineering of Ministry of Education, Beijing University of Technology, Beijing 100124, China

Custom Citation

YANG Liang, YANG Yong-tao, ZHENG Hong, . The phase field numerical manifold method for crack propagation in rock[J]. Rock and Soil Mechanics, 2021, 42(12): 3419-3427.

Rock and Soil Mechanics 2021 42(12): 3419−3427 ISSN 1000−7598
https: //doi.org/10.16285/j.rsm.2021.5556 rocksoilmech.researchcommons.org/journal

The phase field numerical manifold method for crack propagation in rock

YANG Liang[1, 2], YANG Yong-tao[1], ZHENG Hong[3]

1. State Key Laboratory of Geomechanics and Geotechnical Engineering, Institute of Rock and Soil Mechanics, Chinese Academy of Sciences, Wuhan, Hubei 430071, China

2. University of Chinese Academy of Sciences, Beijing 100049, China

3. Key Laboratory of Urban Security and Disaster Engineering of Ministry of Education, Beijing University of Technology, Beijing 100124, China

Abstract: Fracture is one of the most common failure modes of materials and components and greatly restricts engineering design. Understanding of the crack propagation and evolution of rock and other engineering materials is of great significance to engineering construction. For the current numerical methods there are more or less limitations when analyzing the evolution of cracks, such as the mesh dependence of the crack path, the difficulty to deal with crack bifurcation and merging by the classic fracture criterion. In recent years, the phase field method (PFM) has been widely used in simulating crack growth. A phase field numerical manifold method (PFNMM) makes use of the advantages of the phase field method in simulating crack propagation and those of the numerical manifold method (NMM), is proposed for crack growth in rock. The implementation details of the proposed numerical model are presented. Several benchmark examples, including notched semi-circular bend test and Brazilian disc test, are adopted to validate the proposed numerical approach. After that, the multi-crack propagation process with different rock bridge inclination angles under uniaxial compression is simulated, which is in good agreement with the results derived from laboratory and PFC. And the results indicate that the PFNMM has broad application prospects in simulating crack growth of rock.

Keywords: phase field method; variational fracture; numerical manifold method; crack propagation

1 Introduction

After a long period of geological tectonic action, numerous discontinuities with different scales and distributions have developed inside rock, which greatly reduce the mechanical properties of rock mass and increase the difficulty of engineering construction. The research shows that the failure of rock engineering is usually caused by the propagation and coalescence of cracks inside the rock mass. Therefore, the prediction of crack propagation process in rock by numerical methods has always been a research hotspot of scholars around the world.

Nowadays, the common numerical methods for simulating crack propagation include finite element method (FEM), extended finite element method (XFEM), and numerical manifold method (NMM). The early methods used in FEM to solve discontinuous problems mainly include equivalent continuum models[1] and joint elements or interface elements, such as the no-thickness joint elements proposed by Goodman et al.[2]. However, FEM needs constantly remeshing and mapping data when simulating crack growth, which increase the computational difficulty. In order to overcome the shortcomings of FEM in simulating cracks, Belytschko et al.[3−4] proposed XFEM to simulate crack propagation. XFEM uses the level set method to track cracks, avoiding mesh reconstruction in FEM. However, for the complex multi-crack problems, especially the three-dimensional crack propagation problems, it is difficult for XFEM to track the cracks by the level set method. Shi[5] proposed NMM in 1991. The strengths of NMM lie in scaling and cutting, where the scaling technique is able to reproduce local properties and the cutting technique is used to define discontinuities. Therefore, NMM can uniformly deal with continuous/discontinuous problems and is used to simulate crack propagation and other aspects.

Wang et al.[6] used NMM for the first time to simulate rock crack growth, and simulated the single crack growth and crack propagation problem under tension and compression. Peng[7] simulated the dynamic crack propagation problem with the help of NMM. Zhang et al.[8] constructed a high-order NMM for simulating crack propagation. At the same time, Zhang et al.[9] introduced the crack tip asymptotic field into the NMM, and established a calculation method for the interactive integration of the stress intensity factor. Ning et al.[10] adopted the Mohr-Coulomb criterion as the criterion for crack propagation and used NMM to simulate problems such as slope instability. Zheng et al.[11] established a meshless NMM based on moving least squares and simulated multi-crack propagation. Meanwhile, Zheng et al.[12] provided a simple calculation method of numerical integration with $1/r$ singularity

Received: 14 April 2021 Revised: 15 July 2021
This work was supported by the National Natural Science Foundation of China(51538001).
First author: YANG Liang, male, born in 1989, PhD candidate, focusing on computational rock mechanics. E-mail: yangliang18@mails.ucas.ac.cn

function and a more concise description of the progressive displacement field at the tip of a kink crack.

In recent years, the simulation of crack propagation by the phase field method has attracted great attention from scholars around the world. The phase field method for simulating cracks in brittle materials can be traced back to the fracture variational theory proposed by Francfort et al.[13]. Subsequently, Bourdin et al.[14−15] proposed the crack regularization theory, making the phase field method widely used to simulate various crack propagation problems. Miehe et al.[16−17] proposed the strain spectrum decomposition method and the alternate iteration method, which further promoted the phase field method in simulating crack propagation. However, the current phase field methods all solve the crack propagation problem under the finite element framework. The phase field numerical manifold method proposed in this paper combines the advantages of the NMM and the phase field method to simulate the crack propagation problem in rocks.

2 Fracture phase field theory

2.1 Energy minimization theory

In order to better describe the phase field method, a linear elastic solid $\Omega \subset R^n (n \in \{2,3\})$ is taken as the research object, as shown in Fig.1. There is a crack Γ in the problem domain Ω, and the crack width is controlled by l. The problem domain boundary is divided into natural boundary $\partial_N \Omega$ and essential boundary $\partial_E \Omega$, and they satisfy $\partial_N \Omega \cup \partial_E \Omega = \partial\Omega$, $\partial_N \Omega \cap \partial_E \Omega = \varnothing$. There is a fixed displacement constrain $\bar{\boldsymbol{u}}$ on $\partial_E \Omega$. At the same time, the solid Ω is subject to the combination of body force $\boldsymbol{b}$ and surface force $\boldsymbol{f}$. According to the variational fracture theory proposed by Francfort et al.[13], the energy $\Pi(\boldsymbol{\varepsilon}, \Gamma)$ of the system consists of strain energy $\Psi_e(\boldsymbol{\varepsilon}, \Gamma)$ and crack surface energy $\psi_s(\Gamma)$. That is

$$\Pi(\boldsymbol{\varepsilon}, \Gamma) = \Psi_e(\boldsymbol{\varepsilon}, \Gamma) + \Psi_s(\Gamma) \tag{1}$$

where $\boldsymbol{\varepsilon}$ is the strain tensor under the assumption of small deformation.

In order to reflect the anisotropy of rock materials, the strain spectrum decomposition model proposed by Miehe et al.[16−17] is adopted. In this model, the strain energy is decomposed into positive strain energy $\psi^+(\boldsymbol{\varepsilon})$ and negative strain energy $\psi^-(\boldsymbol{\varepsilon})$. And the positive strain energy dissipates with the crack propagation.

$$\Psi_e(\boldsymbol{\varepsilon}, \Gamma) = \int_{\Omega \setminus \Gamma} \left[g(\Gamma)\psi^+(\boldsymbol{\varepsilon}) + \psi^-(\boldsymbol{\varepsilon}) \right] \mathrm{d}\Omega \tag{2}$$

where $g(\Gamma)$ is the dissipation function; $\Omega \setminus \Gamma$ is the region in the problem domain that doesn't contain cracks.

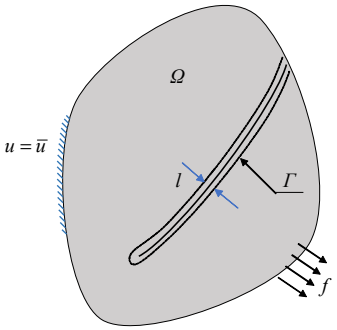

Fig. 1 The linear elastic solid Ω containing a preexisting crack Γ

$$\psi^{\pm}(\boldsymbol{\varepsilon}) = \lambda \mathrm{tr}^2[\boldsymbol{\varepsilon}_{\pm}]/2 + \mu \mathrm{tr}[\boldsymbol{\varepsilon}_{\pm}^2] \tag{3}$$

where λ, μ are the Lame constants.

$$\boldsymbol{\varepsilon} = \boldsymbol{\varepsilon}_+ + \boldsymbol{\varepsilon}_- \tag{4}$$

$$\boldsymbol{\varepsilon}_{\pm} = \sum_{i=1}^{3} \langle \varepsilon^i \rangle_{\pm} \boldsymbol{n}^i \otimes \boldsymbol{n}^i \tag{5}$$

with

$$\langle x \rangle_{\pm} := (x + |x|)/2 \tag{6}$$

The crack surface energy $\psi_s(\Gamma)$ is expressed by

$$\psi_s(\Gamma) = G_c \int_{\Gamma} \mathrm{d}\Gamma \tag{7}$$

where G_c is the critical energy release rate.

The variational fracture theory expounds the crack propagation process from the viewpoint of energy. It is believed that the crack propagation of brittle materials under the action of external force is a process in which the external force potential energy $P(\boldsymbol{u})$ is converted into the strain energy $\Psi_e(\boldsymbol{\varepsilon}, \Gamma)$ stored in the elastic body and the crack surface energy $\Psi_s(\Gamma)$ required for the formation of new cracks. The crack propagation mechanism (crack initiation time, propagation direction, propagation length, etc.) all boils down to the fact that the real displacement field $\boldsymbol{u}$ and the crack field Γ among many permissible displacements and permissible cracks minimize the total energy of the system. That is

$$(\boldsymbol{u}^*, \Gamma^*) = \mathrm{Arg}\{\min \Pi(\boldsymbol{\varepsilon}, \Gamma) - P(\boldsymbol{u})\} \tag{8}$$

where $P(\boldsymbol{u})$ is the external force potential energy.

$$P(\boldsymbol{u}) = \int_{\Omega} \boldsymbol{b} \cdot \boldsymbol{u} \mathrm{d}\Omega + \int_{\partial_N \Omega} \boldsymbol{f} \cdot \boldsymbol{u} \mathrm{d}s \tag{9}$$

However, the biggest difficulty of energy minimization theory lies in the accuracy and appropriacy of description of cracks Γ.

2.2 Smeared crack model

There is an infinitely long rod with crack, as shown in Fig.2(a). The crack filed $d(x) \in [0,1]$ is now introduced

to describe the crack. $d(x)=1$ means complete rupture, while $d(x)=0$ means the material is intact. $d(x)\in(0,1)$ indicates that the material is in a damaged state. If a discontinuous method is used, it can be described by a δ function, as shown in Fig.2(b). Discontinuous cracks correspond to the real situation and are also called sharp cracks or explicit cracks. Miehe et al.[17] proposed to approximate the real crack in the form of an exponential function with the help of the idea of continuity. That is

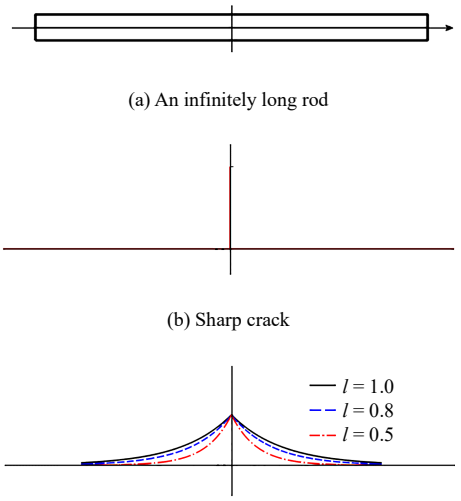

(a) An infinitely long rod

(b) Sharp crack

(c) Smeared crack

Fig. 2 Sharp crack and smeared crack

$$d(x)=\mathrm{e}^{-\frac{|x|}{l}} \tag{10}$$

where l is the crack width, as shown in Fig.2(c). The smaller the crack width l, the narrower the crack, and the closer the crack is to the real crack. In this case, the crack is called an implicit crack or a smeared crack. When $l\to 0$, the exponential function approximates the δ function. That is, smeared cracks are transformed into sharp cracks.

Equation (10) is the solution when the functional (11) takes a stationary value under the constraint of Eq.(12).

$$\Gamma_l(d)=\int_\Omega \frac{1}{2l}(d^2+l^2d'^2)\mathrm{d}\Omega \tag{11}$$

$$\text{s.t.}\begin{cases} d(0)=1 \\ d(\pm\infty)=0 \end{cases} \tag{12}$$

Therefore, the functional formula (11) is used to describe the crack, where $\Gamma_l(d)$ is denoted as the crack surface function. d' is the derivative of the crack phase variable d with respect to space. With equation (11) substituted into Eq.(7), the crack surface energy $\Psi_s(\Gamma)$ can be re-expressed as

$$\Psi_s(\Gamma)=G_c\int_\Omega \frac{1}{2l}(d^2+l^2d'^2)\mathrm{d}\Omega \tag{13}$$

In order to distinguish sharp cracks and smeared cracks, the energy $\Pi(\boldsymbol{\varepsilon},\Gamma)$ after the dispersion description is updated to $\Pi_l(\boldsymbol{\varepsilon},d)$:

$$\Pi_l(\boldsymbol{\varepsilon},d)=\int_{\Omega\setminus\Gamma} g(\Gamma)\psi^+(\boldsymbol{\varepsilon})+\psi^-(\boldsymbol{\varepsilon})\mathrm{d}\Omega+$$

$$G_c\int_\Omega \frac{1}{2l}(d^2+l^2d'^2)\mathrm{d}\Omega \tag{14}$$

Linse et al.[18] proved that $l\to 0$, $\Pi_l(\boldsymbol{\varepsilon},d)\to\Pi(\boldsymbol{\varepsilon},\Gamma)$.

2.3 Governing equation

According to the principle of virtual work, the first-order variation of Eq.(9) can be obtained to obtain the virtual work of external force δW_{ext}:

$$\delta W_{\text{ext}}=\int_\Omega \boldsymbol{b}\cdot\delta\boldsymbol{u}\mathrm{d}\Omega+\int_{\partial_N\Omega}\boldsymbol{f}\cdot\delta\boldsymbol{u}\mathrm{d}s \tag{15}$$

Meanwhile, the first-order variation of Eq.(14) is taken to obtain the virtual work of internal force:

$$\delta W_{\text{int}}=\frac{\partial\Pi_l(\boldsymbol{\varepsilon},d)}{\partial\boldsymbol{\varepsilon}}\delta\boldsymbol{\varepsilon}+\frac{\partial\Pi_l(\boldsymbol{\varepsilon},d)}{\partial d}\delta d \tag{16}$$

$$\delta W_{\text{int}}=\int_{\Omega\setminus\Gamma}\boldsymbol{\sigma}\cdot\delta\boldsymbol{\varepsilon}\mathrm{d}\Omega-\int_\Omega 2(1-d)\delta d\Psi^+(\boldsymbol{\varepsilon})\mathrm{d}\Omega+$$

$$G_c\int_\Omega(l\nabla d\cdot\nabla\delta d+\frac{1}{l}d\delta d)\mathrm{d}\Omega \tag{17}$$

Because of $\delta W_{\text{ext}}-\delta W_{\text{int}}=0$

$$\int_{\Omega\setminus\Gamma}\boldsymbol{\sigma}\cdot\delta\boldsymbol{\varepsilon}\mathrm{d}\Omega-\int_\Omega\boldsymbol{b}\cdot\delta\boldsymbol{u}\mathrm{d}\Omega-\int_{\partial_N\Omega}\boldsymbol{f}\cdot\delta\boldsymbol{u}\mathrm{d}s+$$

$$\int_\Omega -2(1-d)\delta d\Psi^+(\boldsymbol{\varepsilon})\mathrm{d}\Omega+$$

$$G_c\int_\Omega\left(l\nabla d\cdot\nabla\delta d+\frac{1}{l}d\delta d\right)\mathrm{d}\Omega=0 \tag{18}$$

According to the integral by parts and the Gaussian formula, for any $\delta\boldsymbol{u}$ and δd, Eq.(18) holds. Therefore, the displacement field and phase field governing equations are obtained respectively:

$$\nabla\cdot\boldsymbol{\sigma}+\boldsymbol{b}=0 \quad \text{in } \Omega \tag{19}$$

$$\boldsymbol{\sigma}\cdot\boldsymbol{n}=\boldsymbol{f} \quad \text{on } \partial_N\Omega \tag{20}$$

$$\boldsymbol{u}=\bar{\boldsymbol{u}} \quad \text{on } \partial_E\Omega \tag{21}$$

$$\left\{\frac{G_c}{l}+2\Psi^+(\boldsymbol{\varepsilon})\right\}d-G_cl\Delta d=2\Psi^+(\boldsymbol{\varepsilon}) \quad \text{in } \Omega \tag{22}$$

$$\dot{d}\geqslant 0 \tag{23}$$

3 Spatial discretization and solution

3.1 Phase field numerical manifold method

The displacement field and phase field local field of each physical slice are approximated using constant terms. That is

$$\boldsymbol{u}_i^{\text{h}}=\boldsymbol{u}_i \tag{24}$$

$$d_i^{\mathrm{h}} = d_i \tag{25}$$

where $\boldsymbol{u}_i$ and d_i are the local approximation coefficients of the displacement field and the phase field on the ith physical patch, respectively. Then the global approximation of the displacement field $\boldsymbol{u}^{\mathrm{h}}$ in the problem domain Ω and of the phase field d^{h} is expressed as

$$\boldsymbol{u}^{\mathrm{h}} = \boldsymbol{N}_{\mathrm{u}}\boldsymbol{u} \tag{26}$$

$$d^{\mathrm{h}} = \boldsymbol{N}_{\mathrm{d}}\boldsymbol{d} \tag{27}$$

with

$$\boldsymbol{N}_{\mathrm{u}} = \begin{bmatrix} \phi_1 & 0 & \phi_2 & 0 & \phi_3 & 0 \\ 0 & \phi_1 & 0 & \phi_2 & 0 & \phi_3 \end{bmatrix} \tag{28}$$

$$\boldsymbol{N}_{\mathrm{d}} = [\phi_1 \quad \phi_2 \quad \phi_3] \tag{29}$$

ϕ_i is the weight function of the ith physical patch. $\boldsymbol{u}$ and $\boldsymbol{d}$ are local approximations to the physical slice, respectively. That is

$$\boldsymbol{u} = [\boldsymbol{u}_1^{\mathrm{h}} \quad \boldsymbol{u}_2^{\mathrm{h}} \quad \boldsymbol{u}_3^{\mathrm{h}}] \tag{30}$$

$$\boldsymbol{d} = [d_1^{\mathrm{h}} \quad d_2^{\mathrm{h}} \quad d_3^{\mathrm{h}}] \tag{31}$$

The strain and phase field gradient are respectively discretized as

$$\boldsymbol{\varepsilon} = \boldsymbol{B}_{\mathrm{u}}\boldsymbol{u} \tag{32}$$

$$\nabla d = \boldsymbol{B}_{\mathrm{d}}\boldsymbol{d} \tag{33}$$

with

$$\boldsymbol{B}_{\mathrm{u}} = \boldsymbol{L}_{\mathrm{u}}\boldsymbol{N}_{\mathrm{u}} \tag{34}$$

$$\boldsymbol{B}_{\mathrm{d}} = \boldsymbol{L}_{\mathrm{d}}\boldsymbol{N}_{\mathrm{d}} \tag{35}$$

$\boldsymbol{L}_{\mathrm{u}}$ and $\boldsymbol{L}_{\mathrm{d}}$ are respectively expressed as

$$\boldsymbol{L}_{\mathrm{u}} = \begin{bmatrix} \dfrac{\partial}{\partial x} & 0 \\ 0 & \dfrac{\partial}{\partial y} \\ \dfrac{\partial}{\partial y} & \dfrac{\partial}{\partial x} \end{bmatrix} \tag{36}$$

$$\boldsymbol{L}_{\mathrm{d}} = \begin{bmatrix} \dfrac{\partial}{\partial x} \\ \dfrac{\partial}{\partial y} \end{bmatrix} \tag{37}$$

Substituting Eq.(26) and Eq.(27) into the weak forms of Eq.(19) and Eq.(22), we get:

$$\boldsymbol{K}_{\mathrm{u}}\boldsymbol{u} = \boldsymbol{R}_{\mathrm{u}} \tag{38}$$

$$\boldsymbol{K}_{\mathrm{d}}\boldsymbol{d} = \boldsymbol{R}_{\mathrm{d}} \tag{39}$$

where $\boldsymbol{K}_{\mathrm{u}}$ and $\boldsymbol{K}_{\mathrm{d}}$ are the global stiffness matrices of the displacement field and the phase field, respectively. That is

$$\boldsymbol{K}_{\mathrm{u}} = \int_{\Omega} \boldsymbol{B}_{\mathrm{u}}^{\mathrm{T}} \{[(1-d)^2 + k]\boldsymbol{D}_{\mathrm{p}} + \boldsymbol{D}_n\}\boldsymbol{B}_{\mathrm{u}} \mathrm{d}\Omega \tag{40}$$

$$\boldsymbol{R}_{\mathrm{u}} = \int_{\partial_{\mathrm{N}}\Omega} \boldsymbol{N}_{\mathrm{u}}^{\mathrm{T}} \boldsymbol{f} \mathrm{d}s + \int_{\Omega} \boldsymbol{N}_{\mathrm{u}}^{\mathrm{T}} \boldsymbol{b} \mathrm{d}\Omega \tag{41}$$

$$\boldsymbol{K}_{\mathrm{d}} = \int_{\Omega} \left\{ G_{\mathrm{c}} l \boldsymbol{B}_{\mathrm{d}}^{\mathrm{T}} \boldsymbol{B}_{\mathrm{d}} + \left[\frac{G_{\mathrm{c}}}{l} + 2\psi^{+}(\boldsymbol{\varepsilon}) \right] \boldsymbol{N}_{\mathrm{d}}^{\mathrm{T}} \boldsymbol{N}_{\mathrm{d}} \right\} \mathrm{d}\Omega \tag{42}$$

$$\boldsymbol{R}_{\mathrm{d}} = \int_{\Omega} 2\boldsymbol{N}_{\mathrm{d}} \psi^{+}(\boldsymbol{\varepsilon}) \mathrm{d}\Omega \tag{43}$$

Equations (38) and (39) can be solved iteratively by the Newton-Raphson method.

$$\boldsymbol{u}_{n+1} = \boldsymbol{u}_n + [\boldsymbol{K}_{\mathrm{u}}^n]^{-1} \boldsymbol{r}_{\mathrm{u}}^n \tag{44}$$

$$\boldsymbol{d}_{n+1} = \boldsymbol{d}_n + [\boldsymbol{K}_{\mathrm{d}}^n]^{-1} \boldsymbol{r}_{\mathrm{d}}^n \tag{45}$$

where $\boldsymbol{r}_{\mathrm{u}}$ and $\boldsymbol{r}_{\mathrm{d}}$ are the residuals of the displacement field and the phase field, respectively. That is

$$\boldsymbol{r}_{\mathrm{u}} = \int_{\partial_{\mathrm{N}}\Omega} \boldsymbol{N}_{\mathrm{u}}^{\mathrm{T}} \boldsymbol{f} \mathrm{d}s + \int_{\Omega} \boldsymbol{N}_{\mathrm{u}}^{\mathrm{T}} \boldsymbol{b} \mathrm{d}\Omega - \int_{\Omega} [(1-d)^2 + k] \boldsymbol{B}_{\mathrm{u}}^{\mathrm{T}} \boldsymbol{\sigma} \mathrm{d}\Omega \tag{46}$$

$$\boldsymbol{r}_{\mathrm{d}} = \int_{\Omega} 2\boldsymbol{N}_{\mathrm{d}} \psi^{+}(\boldsymbol{\varepsilon}) \mathrm{d}\Omega - \int_{\Omega} \{ G_{\mathrm{c}} l \boldsymbol{B}_{\mathrm{d}}^{\mathrm{T}} \boldsymbol{B}_{\mathrm{d}} d + \left[\frac{G_{\mathrm{c}}}{l} + 2\psi^{+}(\boldsymbol{\varepsilon}) \right] \boldsymbol{N}_{\mathrm{d}}^{\mathrm{T}} d \} \mathrm{d}\Omega \tag{47}$$

3.2 Verification—pure shear test of square plate with cracks

The square plate test with a preset crack is a classic example of crack propagation simulated by the phase field method. In order to verify the feasibility of simulating crack propagation of the method proposed in this paper, the phase field numerical manifold method is used to simulate the process of crack propagation till failure via this example. As shown in Fig.3(a), the side length of the square plate is 1 mm, and there is a preset horizontal crack Γ_0 with a length of 0.5 mm at the left half-height of the square plate. The square plate is fixed at the bottom and subjected to the horizonal right load at the top, leaving the left and right sides free. Fig.3(b) shows the meshing of the numerical manifold method. To reduce the computation cost, the meshes are refined only in areas where cracks are likely to grow. The parameters are chosen as following: elastic modulus E = 210 kN /mm^2, poisson's ratio ν = 0.29. The critical energy release rate G_{c} = 2.7×10^{-3} kN /mm, and the crack widths are taken as l = 0.02 mm and l = 0.007 5 mm, respectively. Displacement increment step Δu = 1×10^{-5} mm.

Figures 4 and 5 describe the crack propagation paths under different displacement loads for l = 0.02 mm and l = 0.007 5 mm, respectively. The crack propagation paths of both crack widths agree well with those obtained by Miehe et al.[17]. By comparison, it is found that the propagation paths of the two crack widths are almost the

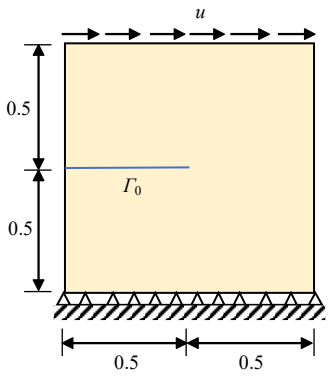

(a) The geometry of model

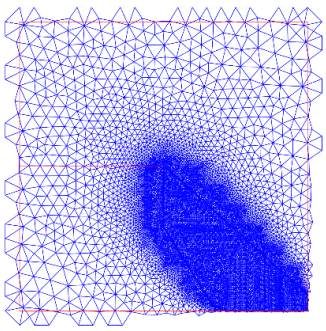

(b) The discrete model

Fig. 3 Test model of pure shear (unit: mm)

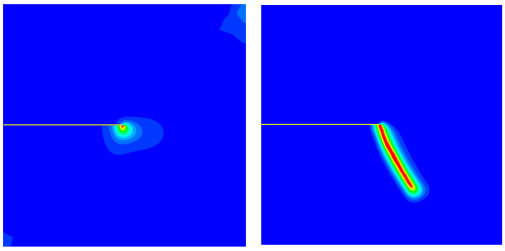

(a) $u = 1.02\times10^{-2}$ mm (b) $u = 1.3\times10^{-2}$ mm

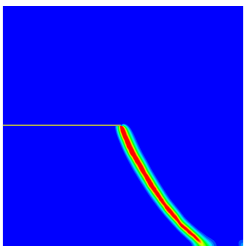

(c) $u = 1.56\times10^{-2}$ mm

Fig. 4 The propagation path of crack at different displacements for l = 0.02 mm

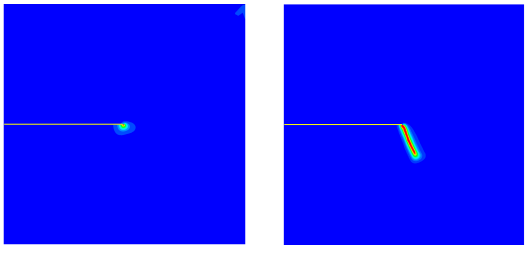

(a) $u = 1.10\times10^{-2}$ mm (b) $u = 1.32\times10^{-2}$ mm

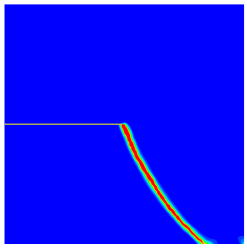

(c) $u = 1.60\times10^{-2}$ mm

Fig. 5 The propagation path of crack at different displacements for l = 0.007 5 mm

same. But the smaller l is, the closer the obtained crack path is to the real crack. Theoretically, when the crack width $l \to 0$, the simulated crack path approximates the real crack. During the crack propagation process, the load−displacement curves are shown in Fig.6. The smaller the crack width l, the larger the maximum shear force the square plate can withstand.

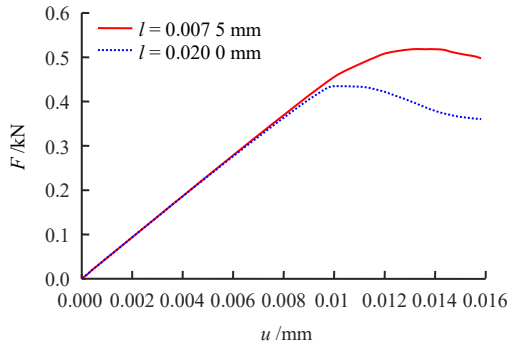

Fig. 6 Load−displacement curves of pure shear

4 Example of rock crack propagation

4.1 The notched semi-circular bend test

The notched semi-circular bend test is a common test method to obtain I-type fracture toughness of rock. The phase field numerical manifold method is used to simulate the experiment. And the ability of the phase field numerical manifold method simulating the crack propagation of rock is verified by comparing the crack paths simulated by the PFNMM and obtained in the experiment.

The geometry model and the mesh model are shown in Fig.7(a), respectively. A crack of length a is prefabricated at the center of the bottom edge of the disc, and a is chosen by 5, 10, and 15 mm, respectively, as shown in Fig.7(b)−7(d). Elastic modulus E = 90 kN /mm^2, Poisson's ratio ν = 0.21, $G_c = 5.6\times10^{-6}$ kN /mm, l = 0.45 mm, $\Delta u = 5\times10^{-6}$ mm.

Figure 8 shows the crack paths obtained by the phase-field numerical manifold method and experiments, respectively. It can be seen that the prefabricated cracks all propagate upward in the vertical direction. The crack

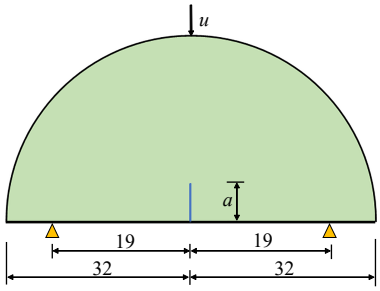

(a) The geometry of model(unit: mm)

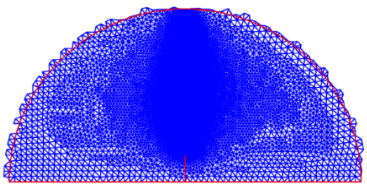

(b) The discrete model for a = 5 mm

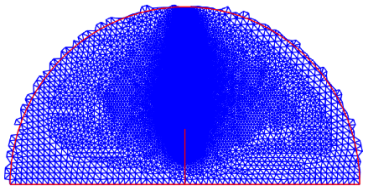

(c) The discrete model for a = 10 mm

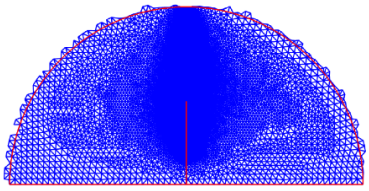

(d) The discrete model for a = 15 mm

Fig. 7 The models of notched semi-circular bend test

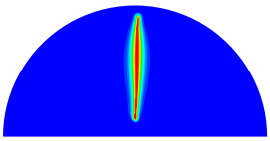

(a) The crack path for a = 5 mm

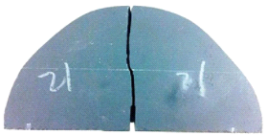

(b) The crack obtained by Lee et al.[19]

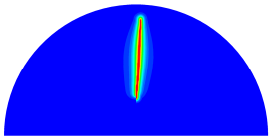

(c) The crack path for a = 10 mm

(d) The crack obtained by Zhao et al.[20]

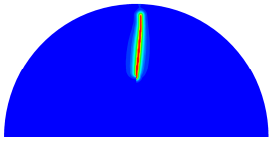

(e) The crack path for a = 15 mm

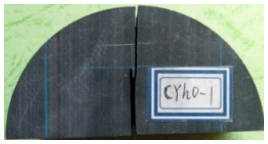

(f) The crack obtained by Zhao et al.[20]

Fig. 8 The crack propagation of notched semi-circular bend test for different lengths of preset crack

propagation path simulated by the phase field numerical manifold method is roughly consistent with the crack propagation trend obtained by the experiment. However, in local details, there are some differences with the experiment results because the calculation model is idealized. Therefore, the numerical simulating cannot completely replace the experiment. The inhomogeneity and anisotropy of the real rock mass raise high demands on the calculation model and numerical method.

Figure 9 records the load-displacement curves during crack propagation. It can be seen that the load−displacement curve increases linearly before the crack initiation but decreases rapidly after the crack initiation until the crack is completely penetrated. Half-disks with different pre-crack lengths can withstand different peak loads. The longer the prefabricated crack is, the smaller the peak load the half-disk can bear.

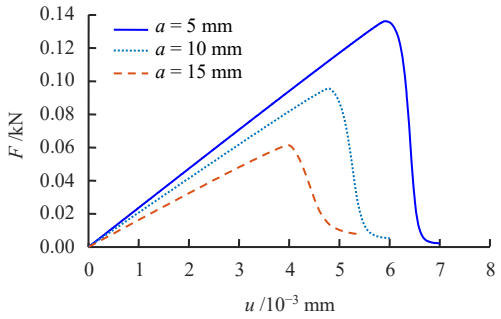

Fig. 9 Load−displacement curves of notched semi-circular bend test

4.2 The Brazilian disc test

The Brazilian disc test is widely used in the engineering field to indirectly determine the tensile strength of brittle rocks. As shown in Fig.10, the Brazilian disk sample with prefabricated cracks has a diameter of 50 mm, an initial crack length of 30 mm, and an angle of 90º between the crack and the horizontal direction.

There is a compression platform at the upper and lower ends of the disc, and the load is applied through the compression platforms at both ends. In this example, the mechanical parameters of the rock sample are E = 10 kN /mm^2, ν = 0.25, G_c = 2.5×10^{-5} kN /mm, l = 1 mm, Δu = 5×10^{-5} mm.

Figure 11 shows the crack paths obtained by the phase field numerical manifold method and by the experiment, respectively. Compared with the experimental results, it can be seen that the crack path obtained by the phase field numerical manifold method is in good agreement with the experimental results. Fig.12 records the change process of the load-displacement curve of the Brazilian disc during

loading. From this figure, it can be seen that the force and displacement are linearly related until the crack propagates. At the initial stage of crack propagation, the force−displacement curve does not drop immediately but appears approximately horizontal. This shows that the load on the disk remains basically unchanged even though the crack starts to propagate. This shows that the friction between the crack surfaces bears part of the load at this moment. As the load continues increasing, the crack gradually expands and coalesces, and the force−displacement curve drops rapidly.

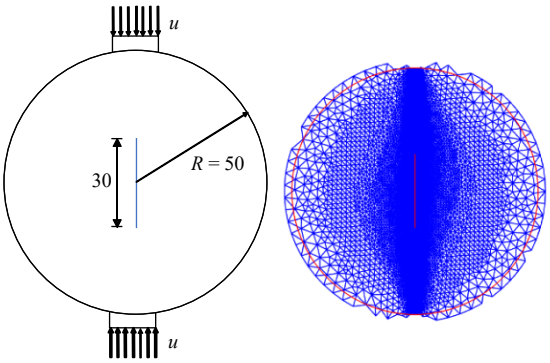

(a) The geometry of model(unit: mm) (b) The discrete model

Fig. 10 The models of Brazilian disc with a crack

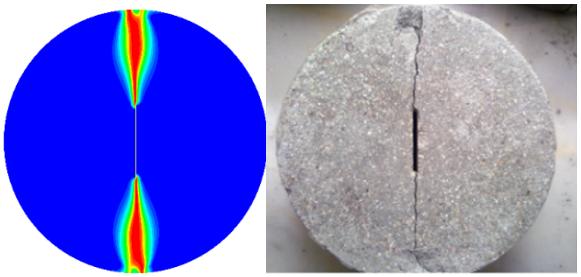

Fig. 11 The crack paths from PFNMM and experiment[21]

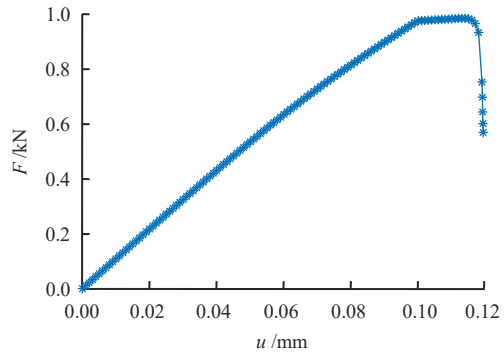

Fig. 12 Load−displacement curves of Brazilian disc test

4.3 Growth of multiple cracks

The first two examples only consider the case of single crack growth, and thus the phase field numerical flow method is used to simulate the growth of multiple cracks. There are two parallel prefabricated cracks in the rectangular rock sample. The two cracks have a spacing of 20 mm and are symmetrical about the centroid of the rectangular rock sample. The crack angle is $\alpha = 45°$, and the rock bridge angle is denoted as β, as shown in Fig.13(a). The crack propagation path under different rock bridge inclination angles is simulated by the phase field numerical manifold method, for which β is equal to 0°, 45°, and 90°, respectively. The grid models of different rock bridge angles are shown in Fig.13(b) to 13(d). In order to compare with the test results[22], the calculation parameters selected for reference test materials are shown in Table 1.

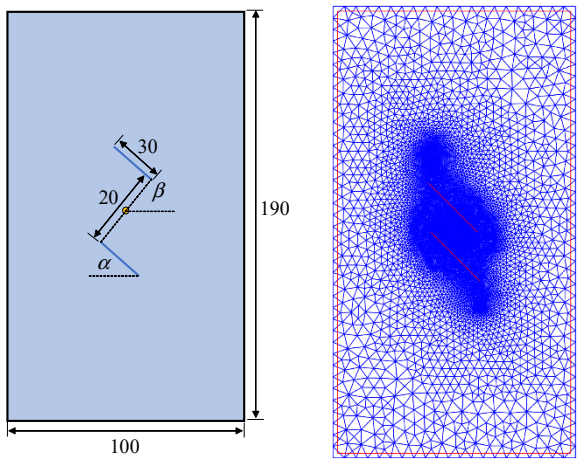

(a) Geometry model (unit: mm) (b) Discretized model for $\beta = 0°$

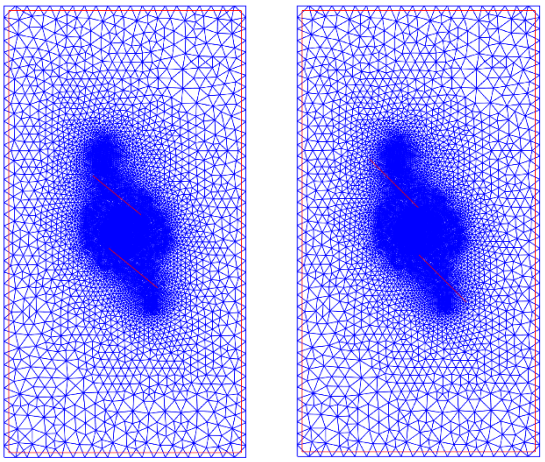

(c) Discretized model for $\beta = 45°$ (d) Discretized model for $\beta = 90°$

Fig. 13 The models of different rock bridge inclination angles

Table 1 The material parameters

Elastic modulus /(kN • mm^{-2})	Poisson's ratio	Critical energy release rate /(kN • mm^{-1})	Crack width /mm
0.67	0.31	1.4×10^{-3}	0.015

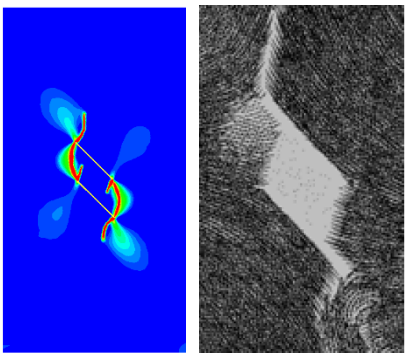

(a) $\beta = 0^{\circ}$

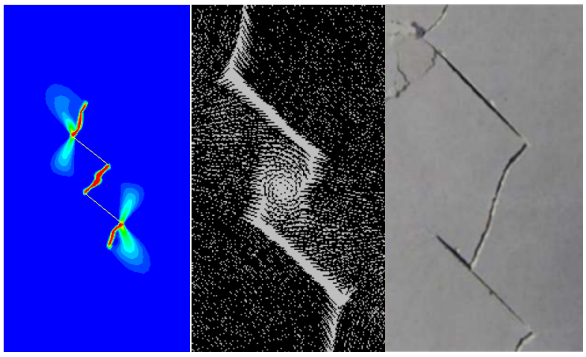

(b) $\beta = 45^{\circ}$

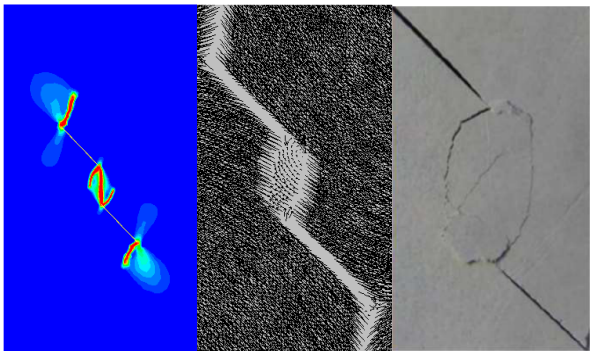

(c) $\beta = 90^{\circ}$

Fig. 14 The crack propagation paths of different rock bridge inclination angles

The crack propagation paths under three different rock bridge inclination angles are shown in Fig.14. In order to verify the path simulated by the phase field numerical manifold method, the comparison with the PFC and experimental results were carried out respectively. As can be seen from Fig.14(a), when $\beta = 0^{\circ}$, the crack propagation paths obtained by the phase field numerical manifold method and particle flow code (PFC) simulations are consistent[22], with airfoil cracks generated at both ends of the prefabricated crack in these two cases. With the increase of the displacement load, the airfoil cracks continue expanding, and the airfoil cracks at the rock bridge end coincide with the prefabricated cracks. Due to the lack of test results of $\beta = 0^{\circ}$ in the study of Yang et al.[22], it cannot be compared with the test. Fig.14(b) successively shows the crack propagation paths obtained by the phase field numerical manifold method, PFC and experiment at $\beta = 45^{\circ}$. It can be seen that the airfoil cracks at the end of the rock bridge intersect. When $\beta = 90^{\circ}$, the crack propagation paths obtained by the three methods are shown in Fig.14(c). From the perspective of airfoil crack propagation, when $\beta = 0^{\circ}$, the propagation angle is the largest, gradually approaching a right angle and extending vertically to both ends of the specimen. That is, it is almost parallel to the maximum principal stress, showing the characteristics of tensile failure. With the increase of β, the airfoil crack propagation angle gradually decreases to about 45°, showing the characteristics of compressive shear failure. It can be seen that the phase field numerical manifold method can better simulate the characteristics of the rock transition from tensile failure to compressive shear failure with the gradual increase of the rock bridge angle.

5 Conclusion

In recent years, the advantages of the phase field method in simulating crack growth have attracted great attention from scholars around the world. In this paper, it is proposed to solve the phase field problem under the framework of the numerical manifold method and to unify the advantages of both. The problem of rock crack propagation is analyzed by numerical examples. The results show:

(1) The phase field numerical manifold method can simulate the crack propagation path well, which is in good agreement with the experimental results.

(2) The phase field numerical manifold method is used to simulate the Brazilian disk test and the notched semi-circular bend test. The load−displacement curve during crack propagation is obtained. When the load is small, crack initiation does not occur, and the load−displacement curve is linear at this moment. The load−displacement curve drops rapidly as the load gradually increases until it reaches the peak value. The load peaks when the crack starts to propagate. With the crack propagation and coalescence, the mechanical properties of the rock decrease rapidly until failure. The load−displacement curve reveals the elastic-brittle failure process of rock.

(3) The phase field numerical manifold method is used to simulate the influence of different rock bridge inclination angles on crack propagation. From the perspective of airfoil crack propagation, when $\beta = 0^{\circ}$, the propagation angle is the largest, and it gradually approaches a right angle and extends vertically to both ends of the

specimen. It is almost parallel to the maximum principal stress, showing the characteristics of tensile failure. With the increase of β, the airfoil crack propagation angle gradually decreases to nearly 45º, showing the characteristics of compression-shear failure. It can be seen that the rock changes from tensile failure to compression shear failure with the gradual increase of the rock bridge inclination angle β. The phase field numerical manifold method is used to simulate the transition from tensile crack to compressive shear crack well.

(4) The research results show the feasibility of the phase field numerical manifold method in studying the failure law of rock materials. Due to the idealization of the computational model, the calculation cannot completely replace the experiment. The inhomogeneity and anisotropy of the real rock mass raise higher requests on the calculation model and numerical method.

References

[1] ZIENKIEWICZ O C, PANDE G N. Time-dependent multi-laminate model of rocks-a numerical study of deformation and failure of rock masses[J]. International Journal for Numerical and Analytical Methods in Geomechanics, 1977, 1(3): 219−247.

[2] GOODMAN R E, JOHN C. Chapter 4: finite element analysis for discontinuous rocks[M]//Numerical Methods in Geotechnical Engineering. [S. l.]: [s. n.], 1977: 148−175.

[3] BELYTSCHKO T, BLACK T. Elastic crack growth in finite elements with minimal remeshing[J]. International Journal for Numerical Methods in Engineering, 1999, 45(5): 601−620.

[4] DOLBOW J, BELYTSCHKO T. A finite element method for crack growth without remeshing[J]. International Journal for Numerical Methods in Engineering, 1999, 46(1): 131−150.

[5] SHI G H. Manifold method of material analysis[C]//Transactions of the 9th Army Conference on Applied Mathematics and Computing. Minneapolis: U. S. Army Research Office, 1992.

[6] WANG Shui-lin, GE Xiu-run. Application of manifold method in simulation crack propagation[J]. Chinese Journal of Rock Mechanics and Engineering, 1997, 16(5): 405−410.

[7] PENG Zi-qiang. The numerical manifold method and simulation of dynamic fracture propagation[D]. Wuhan: Institute of Rock and Soil Mechanics, Chinese Academy of Sciences, 2003.

[8] ZHANG G X, SUGIURA HASEGAWA H. Crack propagation by manifold and boundary element method[C]// ICADD-3: Third International Conference on Analysis of Discontinuous Deformation from Theory to Practice. [S. l.]: [s. n.], 1999: 273−282.

[9] ZHANG H H, LI L X, AN X M, et al. Numerical analysis of 2-D crack propagation problems using the numerical manifold method[J]. Engineering Analysis with Boundary Elements, 2010, 34(1): 41−50.

[10] NING Y J, AN X M, MA G W. Footwall slope stability analysis with the numerical manifold method[J]. International Journal of Rock Mechanics and Mining Sciences, 2011, 48(6): 964−975.

[11] ZHENG H, LI W. The MLS-based numerical manifold method with applications to crack analysis[J]. International Journal of Fracture, 2014, 190(2): 47−166.

[12] ZHENG H, XU D D. New strategies for some issues of numerical manifold method in simulation of crack propagation[J]. International Journal for Numerical Methods in Engineering, 2014, 97(13): 986−1010.

[13] FRANCFORT G A, MARIGO J J. Revisiting brittle fracture as an energy minimization problem[J]. Journal of the Mechanics and Physics of Solids, 1998, 46(8): 1319−1342.

[14] BOURDIN B. Numerical implementation of the variational formulation for quasi-static brittle fracture[J]. Interface Free Bound, 2007, 9: 411−430.

[15] BOURDIN B, FRANCFORT G A, MARIGO J J. Numerical experiments in revisited brittle fracture[J]. Journal of the Mechanics and Physics of Solids, 2000, 48(4): 797−826.

[16] MIEHE C, WELSCHINGER F, HOFACKER M. Thermodynamically consistent phase-field models of fracture: variational principles and multi-field FE implementations[J]. International Journal for Numerical Methods in Engineering, 2010, 83(10): 1273−1311.

[17] MIEHE C, HOFACKER M, WELSCHINGER F. A phase field model for rate-independent crack propagation: robust algorithmic implementation based on operator splits[J]. Computer Methods in Applied Mechanics and Engineering, 2010, 199(45−48): 2765−2778.

[18] LINSE T, HENNIG P, KAESTNER M, et al. A convergence study of phase-field models for brittle fracture[J]. Engineering Fracture Mechanics, 2017, 184: 307−318.

[19] LEE HUNJOO P, OLSON J E, HOLDER J, et al. The interaction of propagating opening mode fractures with preexisting discontinuities in shale[J]. Journal of Geophysical Research: Solid Earth, 2015, 120(1): 169−181.

[20] ZHAO Zi-jiang, LIU Da-an, CUI Zhen-dong, et al. Experimental study of determining fracture toughness KIC of shale by semi-disk three-point bending[J]. Rock and Soil Mechanics, 2018, 39(Suppl.1): 258−266.

[21] HAERI H, SHAHRIAR K, MARJI MF, et al. Experimental and numerical study of crack propagation and coalescence in pre-cracked rock-like disks[J]. International Journal of Rock Mechanics and Mining Sciences, 2014, 67: 20−28.

[22] YANG Qing, LIU Yuan-jun. Simulations of crack propagation in rock-link materials using particle flow code[J]. Chinese Journal of Rock Mechanics and Engineering, 2012, 31(Suppl.1): 3123−3129.